

# Passive Modal Damping with Piezoelectric Shunts

John J. Granier<sup>1</sup>, R. Jason Hundhausen<sup>2</sup>, Gabriel E. Gaytan<sup>3</sup>

<sup>1</sup>Dept. of Mechanical Engineering, Texas Tech. University, Lubbock

<sup>2</sup>Dept. of Mechanical Engineering, Montana State University, Bozeman

<sup>3</sup>Dept. of Civil Engineering, University of California, Irvine

## ABSTRACT

The use of piezoelectric materials in conjunction with passive inductance-resistance-capacitance (RLC) circuits to dampen specific vibration modes is explored. The piezoelectric materials convert mechanical energy to electrical energy, which is then dissipated in the RLC circuit through joule heating. An impulse is applied to a simple cantilevered beam and by varying the inductance and resistance values, the natural oscillation frequency for the RLC circuit is tuned to dampen the first mode of vibration.

## NOMENCLATURE

C	capacitance
E	modulus of Elasticity
f	frequency
h	dimension along z-axis (height)
i	current
I	moment of Inertia
$k_{31}$	transverse coupling coefficient
$K_{31}$	generalized electromechanical coupling coefficient
l	dimension along x-axis (length)
L	inductance
m	mass
M	moment
P	electrical power
R	dissipation tuning parameter
R	electrical resistance
t	time variable
U	strain energy
V	voltage
w	dimension along z-axis (width)
y	free end beam displacement
Y	initial condition of y

### Greek

$\alpha$	normalized tuning frequency
$\phi$	phase angle
$\rho$	density
$\omega$	natural frequency

$\lambda$	dimensionless parameter determined by boundary conditions
$\sigma$	dimensionless parameter determined as a function of $\lambda$
$\zeta$	zeta, damping ratio ( $c/c_c$ )

### Subscripts

e	electrical
n	natural frequency
i	mode index
o	open circuit
s	short circuit
S	series configuration
opt	optimum
P	parallel configuration
PZT	referring to piezoelectric patches

### Superscript

s	constant strain, post-bonded
T	prebonded

## INTRODUCTION

Structural damping is an important means of reducing vibration, noise and fatigue. Vibration can be suppressed by adding mass to a system, introducing a mechanical vibration absorber or a variety of other techniques. This paper explores the use of “smart materials” or piezoelectric polymers in conjunction with an electrical shunt circuit as a single mode damper.

Piezoelectric materials have the unique ability to convert mechanical energy into electrical energy and vice versa. When strained, piezoelectric materials produce a voltage difference across the poled terminals. This characteristic has been exploited in various configurations of mechanical sensors. Inversely, piezoelectric materials strain when a voltage is applied. This characteristic enables piezoelectric materials to be used as mechanical actuators.

Hagood and von Flotow (1991) [2] analytically predicted and experimentally proved the effectiveness

of piezoelectric materials and passive shunt circuits to damp a single mode of vibration. The theory was then expanded by Hollkamp (1994) [3] to use passively shunted piezoelectric materials as a bi-modal damper. Active control systems require complex amplifiers and electronic sensors. Implementation of simple and robust passive control systems using piezoelectric materials decreases the risk of malfunction and deterioration.

A passive control system is used to damp a single mode of a simple cantilever beam (1-DOF). Analysis was done to predict the optimal position of a piezoelectric tile on the beam. A resonant shunt circuit was created using an inductor and resistor in series and parallel. The electrical impedance frequency was tuned to equate the modal frequency that was to be damped.

### THEORY (Cantilever Beam)

An analytical model has been developed to determine point displacements, mode shapes and strain energy of a cantilever beam. A beam clamped at one end and free at the other was used. Figure 1 illustrates the beam variable dimensions and free-end displacement

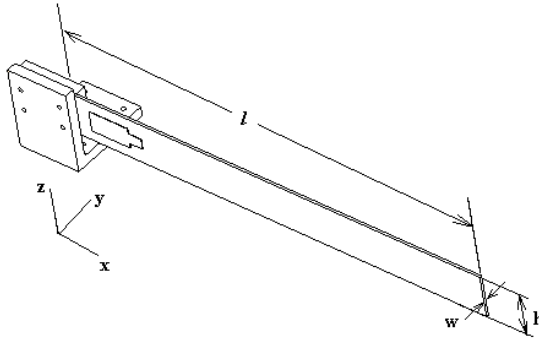


Figure 1: Cantilever Beam Schematic

An ideal cantilever beam with zero damping ( $\zeta = 0$ ) will oscillate with harmonic motion. The displacement of the free end can be recorded as a function of time as [5]

$$y_{\zeta=0} = Y \sin(\omega_n t) \quad (1)$$

with  $\omega_n$  defined as the natural frequency and the amplitude ( $Y$ ) is dependent on the driving force. The underdamped behavior ( $\zeta < 1.0$ ) can be expressed by the exponential decay function [5]

$$y = Y e^{-\zeta \omega_n t} \sin(\sqrt{1 - \zeta^2} \omega_n t + \phi) \quad (2)$$

The phase angle ( $\phi$ ) is determined by the initial conditions.

Cantilever beam mode shapes can be determined using Equation 3 [1].

$$\tilde{y}_i = \cosh \frac{\lambda_i x}{l} - \cos \frac{\lambda_i x}{l} - \sigma_i \left( \sinh \frac{\lambda_i x}{l} - \sin \frac{\lambda_i x}{l} \right) \quad (3)$$

$\lambda_i$  and  $\sigma_i$  are dimensionless parameters that are a function of the beam's boundary conditions. The natural frequency for each mode ( $i$ ) can be determine by

$$f_i = \frac{\lambda_i^2}{l^2} \sqrt{\frac{EI}{m}} \quad \{\text{rad/s}\} \quad (4)$$

The strain energy per unit length was analyzed to predict the optimal bonding location of the piezoelectric tiles. Total strain energy can be computed by [5]

$$U = \frac{1}{2} \int EI \left( \frac{d^2 y}{dx^2} \right)^2 dx \quad (5)$$

The moment applied as a function of position along the beam is

$$M(x) = \frac{d^2 y}{dx^2} \quad (6)$$

The strain energy as a function of position along the beam is

$$U(x) = \frac{1}{2} EI * M(x)^2 \quad (7)$$

### Piezoelectric Materials

A piezoelectric material is a three-dimensional device poled along one axis. Most piezoelectric patches (PZT) are poled across the thickness with electrodes through the top and bottom planes. As a voltage difference is applied across the electrodes ( $x_3$  direction in Figure 2), a strain is produced in the other two directions ( $x_1$  and  $x_2$ ).

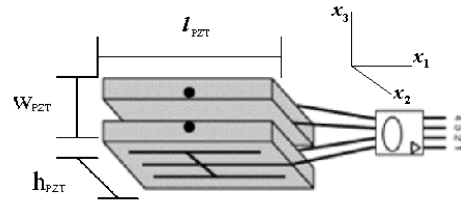


Figure 2: Piezoelectric (Bimorph) Patch Design

For the given experiment, axis 1 is bonded along the horizontal neutral axis of the cantilever beam as shown in Figure 1. When deformed by the cantilever bending, the PZT produces a voltage across axis 3. The material transverse coupling constant ( $k_{ij}$ ) is used to describe the relationship of energy transfer from the  $i$ -axis to the  $j$ -axis and is specific to the PZT patch

design. The experiment was conducted and analyzed in mode 31.

A simplified description of the PZT damper is to convert mechanical energy into electrical energy and then dissipate the electrical energy in the form of joule heating through a resistor. The equation for power dissipated by the resistor is

$$P = i^2 R = \frac{V^2}{R} \quad (8)$$

Maximizing the current through the resistor increases electrical damping.

A simple resistor shunt circuit can be used as a broadband damper. The resistor will effectively dissipate energy from all modes of vibration.

#### Parallel RL Circuit

An inductor-resistor shunt circuit was implemented to create an electrical resonant frequency for single mode damping. Placing the inductor and resistor in parallel to the PZT allows for the simplest electrical frequency tuning because the inductor and resistor can be altered independently. Optimum resistor and inductor values for a parallel configuration were calculated using the method outlined by Wu and Bicos (1997) [6].

1. Experimentally determine  $\omega_o$  and  $\omega_s$  for the cantilever beam.  $\omega_o$  and  $\omega_s$  are the PZT open-circuit and short-circuit modal frequencies for the cantilever beam.
2. Calculate the generalized electromechanical coupling coefficient for mode 31.

$$K_{31} = \sqrt{(\omega_o^2 - \omega_s^2) / \omega_s^2} \quad (9)$$

3. Determine the PZT capacitance at constant strain.  $C^T$  is the pre-bonded PZT capacitance.

$$C^s = (1 - k_{31}^2) C^T \quad (10)$$

4. Calculate the normalized tuning frequency

$$\alpha = \sqrt{(1 - K_{31}^2 / 2)} \quad (11)$$

5. The optimum parallel inductance is

$$L_{opt-P} = 1 / [C^s (\omega_s \alpha)^2] \quad (12)$$

6. The optimum parallel shunt resistance is

$$R_{opt-P} = 1 / [\sqrt{2} * \omega_s C^s K_{31}] \quad (13)$$

The disadvantage of the parallel circuit configuration is that a current divider is created and current through the resistor is decreased.

#### Series RL Circuit

By Kirchoff's law, current is constant through elements in series. Therefore, a resistor and

inductor in series with the PZT can achieve maximum current through the resistor. The optimum resistor and inductor values for the series circuit were calculated following the procedures of Hagood and Von Flotow (1991) [2].

The generalized electromechanical coupling coefficient ( $K_{31}$ ) was calculated according to Equation (9). The dissipation tuning parameter was calculated by

$$r = RC^s \omega_o \quad (14)$$

The optimal circuit damping was determined by

$$r_{opt} = \sqrt{2} * K_{31} / (1 + K_{31}^2) \quad (15)$$

Combining Equations 14 and 15 the optimal series shunt resistance is

$$R_{opt-S} = r_{opt} / C^s \omega_o \quad (16)$$

The electrical resonance frequency is

$$\omega_e = \frac{1}{\sqrt{LC^s}} \quad (17)$$

The optimal series configuration inductance value can be calculate by setting the electrical frequency equal to the short-circuit frequency ( $\omega_e = \omega_o$ ).

$$L_{opt-S} = \frac{1}{C^s \omega_s^2} \quad (18)$$

## EXPERIMENTAL DESIGN

A thin aluminum beam was clamped to a stainless steel right angle (shown in Figure 1). The dimensions and material properties of the aluminum beam are shown in Table 1.

Table 1: Aluminum Beam Dimensions and Properties

Aluminum 6061 T651		
	Dimension	Units
length	<i>l</i>	0.535 m
width	<i>w</i>	0.003 m
height	<i>h</i>	0.052 m
Property		
Young's modulus	<i>E</i>	6.90E+10 Pa
Density	<i>r</i>	2700 kg/m <sup>3</sup>

One bimorph piezoelectric patch was bonded on each side of the beam. The PZT manufacturer was ACX model QP25N. Figure 2 is a schematic of the bimorph design. The peizo wafer dimensions and other device properties are shown in Table 2.

Table 2 PZT Dimensions and Properties

ACX model QP25N		
	Dimension	Units
length	$l_{PZT}$	45.974 mm
width	$w_{PZT}$	0.127 mm
height	$h_{PZT}$	20.574 mm
Property		
Capacitance	$C^T$	0.20 mF
Coupling Coefficient	$k_{31}$	0.40
Elastic Modulus	$E_{11}$	6.30E+10 Pa
Elastic Modulus	$E_{33}$	5.00E+10 Pa

## ANALYTICAL SOLUTION

Based on the dimensions and material properties the cantilever beam, mode shapes and modal frequencies were determined using Equations 3 and 4 respectively. These are illustrated in Figure 3 and summarized in Table 3.

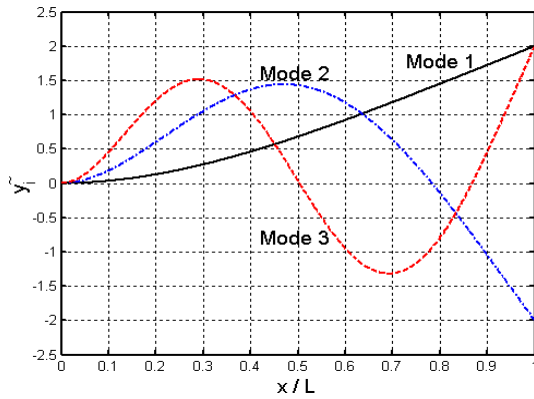


Figure 3: Cantilever Beam Mode Shapes

Table 3: Modal Parameters and Analytical Frequencies

Mode	1	2	3
$\lambda_i^1$	1.87510407	4.69409113	7.85475744
$\sigma_i^2$	0.73409551	1.01846732	0.99224497
$f_i$ [Hz]	8.56	53.64	150.19
$\omega_{n-i}$ [rad/s]	53.78	337.03	943.69

<sup>1</sup>Transcendental equation for  $\lambda$ :  $\cos \lambda \cosh \lambda + 1 = 0$

<sup>2</sup>Equation for  $\sigma$ :  $\frac{\sinh \lambda - \sin \lambda}{\cosh \lambda + \cos \lambda}$

Equation 7 was used to analyze the strain energy throughout the beam for each mode. Figure 4 shows that the maximum strain energy for each of the first three modes occurs at the clamped boundary of the cantilever beam. For this reason the PZT patches were bonded 17mm from the

clamped end on each side of the aluminum beam.

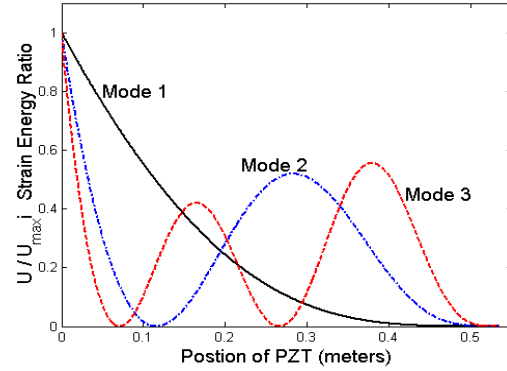


Figure 4: Modal Strain Energy

Law (1996) [6] proved that the analytical equations for strain energy could be used to accurately predict the optimum position of the PZT. Law also shows that analytical models cannot accurately determine the piezoelectric material behavior and damping ability.

## EXPERIMENTAL SOLUTION

A modal hammer with a rubber tip induced a broad band of lower vibration frequencies. The time response data of the beam tip acceleration was analyzed to determine the inherent structural damping in the aluminum material and clamped joint. A PCB accelerometer with 10mV/g sensitivity was used to measure the beam tip acceleration. A Hilbert transform was used to calculate the envelope of peaks of the time response plot (shown in Figure 5).

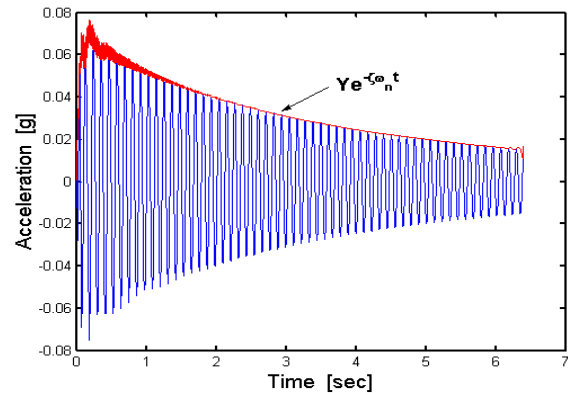


Figure 5: Time Response Plot with Hilbert Envelope

The initial 10% and final 10% of the envelope were neglected to ignore initial conditions and transform inaccuracies. A linear curve fit shown in Fig. 6 was developed from the natural log of the Hilbert envelope.

$$m = \ln(Y e^{-\zeta \omega_n t}) = -\zeta \omega_n t \quad (19)$$

$$\zeta = -m / \omega_n \quad (20)$$

Based on the linear slope,  $\zeta$  was calculated to be 0.415 %.

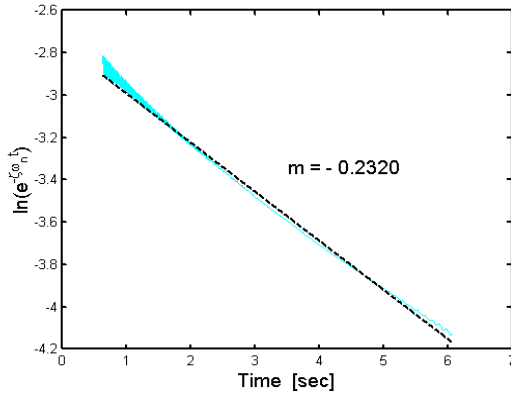


Figure 6: Hilbert Envelope with Linear Approximation

The frequency response function was computed from the time response data to determine the modal frequencies. The natural frequencies were determined to be 8.750, 54.69, and 149.8 for modes 1, 2 and 3 respectively. The experimental modal frequencies are only 2.25% greater than the analytical predictions.

Once the piezoelectric materials were attached, the open and short-circuit frequencies were determined for the first fundamental mode to be 8.750 and 8.9062 Hz respectively as shown in Fig. 7.

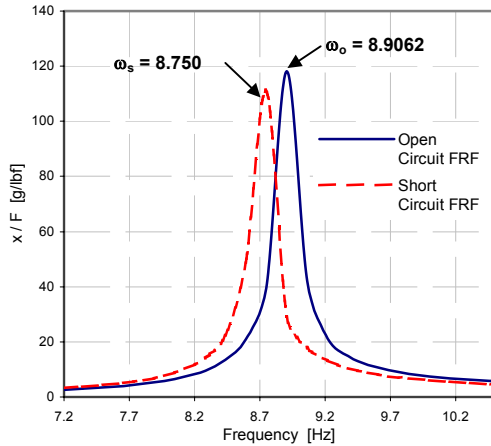


Figure 7: Mode 1 Frequency Response Function

### Parallel Shunting

The initial shunt circuit design was the resistor and inductor in parallel due to the ease of tuning the electrical resonant frequency. Table 4 shows the calculation results of Equations 9 through 13 for the RL parallel circuit configuration.

Table 4: RL Parallel Circuit Values

$\omega_o$	55.958	rad/s
$\omega_s$	55.978	rad/s
$K_{31}$	0.186	
$C^s$	0.168	$\mu\text{F}$
$\alpha$	0.9913	
$L_{\text{opt-P}}$	1933	Henry
$R_{\text{opt-P}}$	404246	$\Omega$

Due to the large inductance required, a synthetic inductor was created as shown in the diagram below. A 741 op-amp was used with a 30 volt DC supply. The synthetic inductance value is determined by

$$L = R_1 R_2 C \quad (21)$$

$R_2$  is shown as a trim pot variable resistor in Fig. 8 to allow precise tuning of the electrical resonant frequency.

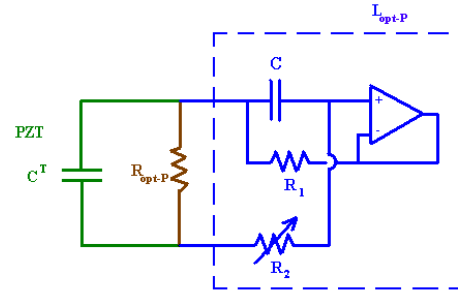


Figure 8: Parallel Circuit with Synthetic Inductor

The parallel circuit configuration was ineffective in significantly decreasing the beam vibration. Various hypotheses for the parallel circuit failure are addressed in the conclusions section.

### Series Shunting

The capacitance ( $C^s$ ) for each of the two PZT patches was measured to determine  $R_{\text{opt-S}}$  and  $L_{\text{opt-S}}$ . The PZT patches will be denoted as PZT-1 and PZT-2 denoting closest to the stainless steel base member and closest to the stainless steel vertical member, respectively. A separate series shunt circuit was created for PZT-1 and PZT-2 because of the varying capacitance values. Shunt circuit parameters are summarized in Table 5.

Table 5: RL Series Shunt Circuit Values

Shunt Parameters	PZT-1		PZT-2	
	$C^s$	158.4	156.6	nF
	$r_{\text{opt}}$	0.4876	0.4876	
	$R_{\text{opt-S}}$	54062	54683	$\Omega$
	$L_{\text{opt-S}}$	2088	2112	Henry

A synthetic inductor was created by the same design shown in Figure 8. Figure 9 shows the series circuit

configuration. The synthetic inductance value is given by Equation 21.

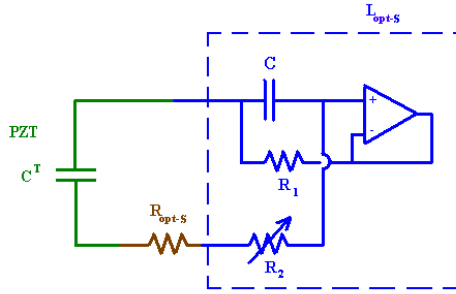


Figure 9: Series Circuit with Synthetic Inductor

Individually shunting each PZT with a series RL circuit increased the damping by 40% from the inherent damping.

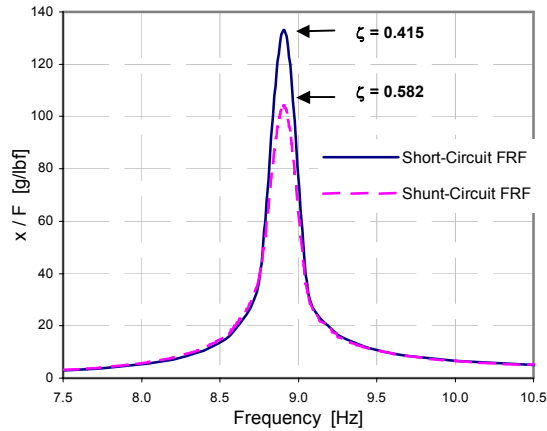


Figure 10 Mode 1 Series RL Circuit Shunting

## CONCLUSIONS

Many difficulties were encountered throughout the course of the experiment. The first problem was an inconsistency in determining  $\omega_0$  and  $\omega_s$ . The values of  $\omega_0$  and  $\omega_s$  would vary depending on the magnitude of the hammer strike. The lack of repeatability and inaccuracy of  $\omega_0$  and  $\omega_s$  can be explained by two hypotheses:

Hypothesis 1: The localized stiffness created by the open-circuit PZT was insignificant in proportion to the remainder of the aluminum beam. The additional stiffness of the PZT was not large enough in magnitude to shift the fundamental frequency of the entire mechanical system.

Hypothesis 2: The resolution of the data acquisition software was not precise enough to record the fractional frequency shift. The

software and available RAM would not allow a larger sampling rate for the needed time interval to prevent aliasing in the FRF plot. Therefore, the fundamental frequencies could only be estimated to the nearest frequency resolution.

The uncertainty of  $\omega_0$  and  $\omega_s$  is sure to be a crucial factor in the inaccuracy of the series and parallel shunt circuit values.

The ineffectiveness of the parallel shunt circuit is contributed to the RL current divider. The impedance of the synthetic inductor was much higher than the impedance of the resistor. Therefore, the current flow was almost completely through the resistor and an electrical resonant frequency was not created. As discussed in the theory section, the parallel circuit configuration was thought to act as a single resistor and a broadband multimode damper. Similar to hypothesis 1, the PZTs used were not efficient enough for the cantilever design to significantly increase multimode damping. The energy converted by the PZTs and dissipated by the resistor was not significant in proportion to the inherent structural damping. The inherent structural damping is mainly attributed to the non-perfectly clamped boundary condition and the aluminum material properties.

As discussed in the theory, the series shunt circuit was more effective because current through the resistor was maximized. The shunt parameters shown in Table 5 were used to build the initial circuits. A trim pot variable resistor was used in the synthetic inductor to fine-tune the electrical resonant frequency.

Based on the results seen by Hagood and von Flotow (1991) [2] the peak amplitude of the shunt circuit FRF shown in Figure 10 was expected to be much lower. The optimum circuit values were expected to increase  $\zeta$  by 80%.

Suggestions for further experimentation include:

1. Implement a more rigid clamped boundary condition to decrease inherent damping.
2. Use a longer cantilever beam or apply a larger deflection to increase strain seen by the PZTs thereby, increasing the available dissipation energy.
3. Tune the shunt circuits to damp mode 2. The higher frequency value requires a smaller inductance.
4. Use multiple single layer piezoelectric patches rather than bimorph patches to simplify wiring and electric circuit designs.

## ACKNOWLEDGEMENTS

The authors would like to thank Amy Robertson for research mentoring and Chuck Farrar the director of Los Alamos Dynamic Summer School program

Funding for the Los Alamos Dynamics Summer School was provided by the Engineering Science and Applications Division at the Los Alamos National Laboratory and the Dept. of Energy's Education Programs Office. The following companies provided data acquisition hardware and various software packages that were necessary to complete the student projects: Dactron, Inc. (data acquisition hardware), Vibrant Technologies (experimental modal analysis software), The Mathworks, Inc. (numerical analysis software), and ANSYS, Inc. (finite element software).

## REFERENCES

1. Blevins, R. D., Formulas for Natural Frequency and Mode Shape, 1995, Kreiger Publishing Company, Malabar, Florida.
2. Hagood N. W., von Flotow, A., 1991, "Damping of Structural Vibrations with Piezoelectric Materials and Passive Electrical Networks", *J. of Sound and Vibration*, Vol. 146(2), pp.243-268.
3. Hollkamp, J. J., 1994, "Multimodal Passive Vibration Suppression with Piezoelectric materials and Resonant Shunts", *J. of Intelligent Material Systems and Structures*, Vol. 5, pp.49-56.
4. Law, H. H., Rossiter, P. L., Simon, G. P., Koss, L. L., 1996, "Characterization of Mechanical Vibration Damping by Piezoelectric Materials", *J. of Sound and Vibration*, Vol. 197(4), pp.489-513.
5. Thomson, W. T., Theory of Vibrations with Applications, Third Edition, 1988, Prentice Hall, Englewood Cliffs, New Jersey.
6. Wu, S and Bicos, A. S., 1997, "Structural vibration damping experiments using improved piezoelectric shunts", *SPIE* Vol. 3045 pp.40-50.